第 54 卷第 2 期
2026 年 2 月

硅 酸 盐 学 报
JOURNAL OF THE CHINESE CERAMIC SOCIETY

Vol. 54，No. 2
February，2026

http://jccsoc.cbpt.cnki.net

DOI：10.14062/j.issn.0454-5648.20250514

Fe 位 Co 掺杂 Fe_2VAl 全哈斯勒合金的热电磁性能

周 龙[1]，余 健[2]，梁 栋[1]，叶先峰[1]，贺丹琪[1]，聂晓蕾[1]，魏 平[1]，赵文俞[1]，张清杰[1]

(1. 武汉理工大学材料复合新技术国家重点实验室，武汉 430070；2. 九江学院材料科学与工程学院，江西 九江 332005)

摘 要：热电磁材料是新型热电/磁卡复合制冷技术的关键材料，但目前常用的磁卡/热电复合材料存在异质界面扩散反应恶化综合性能的问题，研制具有本征热电磁性能的单相材料对推动该技术发展具有重要意义。本研究采用电弧熔炼方法制备了系列名义组成为 $Fe_{2-x}Co_xVAl$ (x=0, 0.5, 1.0, 1.5, 2.0)的全哈斯勒合金，系统研究了 Co 掺杂对其物相组成、磁热性能和热电性能的影响。结果表明，所有 $Fe_{2-x}Co_xVAl$ 合金均为单相材料，Fe 位 Co 掺杂可以显著提高 $Fe_{2-x}Co_xVAl$ 合金的居里温度，x=1.5 和 2.0 样品的居里温度分别提高到 210 K 和 287 K，在 2.5 T 磁场下的最大磁熵变分别为 1.04 J $kg^{-1}\cdot K^{-1}$ 和 0.81 J $kg^{-1}\cdot K^{-1}$；发现 Co 掺杂可同时显著提升电导率和 Seebeck 系数，同时晶格热导率明显下降，材料 zT 大幅提升；x=0.5 样品的最大 zT 在 600 K 时达到 0.073，比 Fe_2VAl 基体提高了 260 倍。表明 Fe 位 Co 掺杂可以协同调控 Fe_2VAl 基全哈斯勒合金的磁热性能和热电性能。

关键词：热电磁材料；全哈斯勒合金；磁热性能；热电性能
中图分类号：TB34　　**文献标志码**：A　　**文章编号**：0454–5648(2026)02–0353–09
网络出版时间：2026–01–26

自 21 世纪以来，全球制冷需求日益增加，传统蒸汽压缩通过压缩制冷剂实现制冷，不仅能耗大，还会产生温室气体排放和臭氧层破坏等一系列环境问题，发展新型绿色制冷技术替代传统压缩制冷对实现“双碳”目标具有重要意义[1–3]。近年来，热电制冷和磁制冷两种全固态制冷技术因尺寸小、可靠性高、无污染等特点而被广泛关注[4–7]。热电制冷基于材料的 Peltier 效应，利用热电材料在电场作用下实现热传递达到制冷效果[8]。热电制冷效率由材料热电优值(zT)决定($zT=\frac{\alpha^2\sigma}{\kappa_C+\kappa_L}T$，其中 α、σ、T、κ_C 和 κ_L 分别表示 Seebeck 系数、电导率、绝对温度、载流子热导率和晶格热导率，$\alpha^2\sigma$ 为功率因子)，zT 越大，制冷系数越高。但由于材料中电–声输运的强耦合效应，室温 zT 值难以突破 2.0，导致热电制冷的应用局限于车载冰箱和便携式空调等小规模领域[9–11]。磁制冷利用磁卡材料的磁热效应，通过等温磁化和绝热去磁过程的反复循环实现制冷[12–14]。理论上磁制冷具有接近卡诺循环的高制冷效率[15]，但目前大多数磁制冷系统采用主动式磁回热器，磁卡材料与磁流体工质间的热量交换主要为固–液交换，热交换效率低和回热损失大导致磁制冷的应用受到严重限制[16–19]。

近年，国内学者提出了一种新型热电/磁卡复合制冷技术，该技术结合热电制冷和磁制冷，利用热电制冷响应速度快和磁制冷理论制冷效率高的优势，有望实现更高的制冷效率[20–22]。实现该技术突破的关键之一在于研制同时具有高热电性能和大磁熵变的热电磁关键材料。复合高 zT 的热电材料和大磁熵变的磁卡材料是制备高性能热电磁材料的常用方法。如 Li 等[23]制备的 1.0% (质量分数，下同) MnCoGe/BiSbTe 复合材料，300 K 时 zT 可达 0.68，2.0 T 时最大磁熵变(ΔS_{max})取得 0.0043 J·$kg^{-1}\cdot K^{-1}$，Liu 等[24]制备的 20%$LaFe_{10.4}Co_{0.8}Si_{1.8}$/$Bi_{0.5}Sb_{1.5}Te_3$ 复合材料在 300 K 时 zT 达 0.46，在 2.5 T 时ΔS_{max} 达 0.81 J·$kg^{-1}\cdot K^{-1}$，Zhu 等[25]研制的 15%Cr_5Te_6/$Bi_{0.4}Sb_{1.6}Te_3$

收稿日期：2025–06–30。　修订日期：2025–07–16。
基金项目：国家自然科学基金项目(52130203，92463310，52201256)。
第一作者：周 龙(2000—)，男，硕士研究生。
通信作者：余 健(1987—)，男，博士，副教授；
魏 平(1984—)，男，博士，教授。

Received date: 2025–06–30.　**Revised date:** 2025–07–16.
First author: ZHOU Long (2000–), male, Master candidate.
E-mail: 345359@whut.edu.cn
Correspondent author: YU Jian (1987–), male, Ph.D., Associate Professor;
WEI Ping (1984–), male, Ph.D., Professor.
E-mail: yujian@jju.edu.cn; pingwei@whut.edu.cn

复合材料在 300 K 时 zT 为 0.65，5 T 时 ΔS_{max} 可达 0.33 $J·kg^{-1}·K^{-1}$。尽管复合热电磁材料可以同时发挥热电材料和磁卡材料的优势，但异质界面处易发生扩散反应，恶化材料性能。如 Wei 等[26]发现制备 Gd/$Bi_{0.5}Sb_{1.5}Te_3$ 过程中，烧结过程中 Gd 和 $Bi_{0.5}Sb_{1.5}Te_3$ 异质界面会形成 Gd–Te 扩散层，明显降低 Gd/$Bi_{0.5}Sb_{1.5}Te_3$ 复合材料的热电性能和磁热性能。因此，研制兼具高热电性能和磁热性能的单相本征热电磁材料，避免复合热电磁材料中的异质界面反应，对推动高效热电磁制冷技术发展具有重要作用。

Fe_2VAl 基全哈斯勒合金由于其独特的电子结构，在室温附近容易获得较高的功率因子，而掺杂异质原子增强声子散射可显著降低晶格热导率，可获得较高的 zT[27]。根据 Slater–Pauling 规则(S–P 规则)可知，完全有序的 Fe_2VAl 是一种非磁性合金[28, 29]。Co 基全哈斯勒合金具有优异的热稳定性和高的居里温度(T_C)，在永磁体、自旋电子学等领域具有巨大应力潜力[30, 31]。在 Fe_2VAl 晶格中引入 Co 元素有望协同调控 Fe_2VAl 基合金的磁热性能与热电性能。本研究采用电弧熔炼方法制备了系列名义组成为 $Fe_{2-x}Co_xVAl$ (x=0, 0.5, 1.0, 1.5, 2.0)的合金，系统研究了 Co 掺杂对其物相组成、显微结构、磁热性能和热电性能的影响。

1 实验

1.1 材料制备

以高纯单质 Fe (99.99%，块状)，Co (99.9%，片状)，V (99.95%，片状)和 Al (99.99%，颗粒状)为原料，采用电弧熔炼在氩气环境中制备了系列名义组成为 $Fe_{2-x}Co_xVAl$ (x=0, 0.5, 1.0, 1.5, 2.0)的合金铸锭。为确保合金的均匀性，合金铸锭均熔炼 5 次，并在每次重熔前翻转铸锭。采用电火花线切割加工设备将所得铸锭切割成特定块体形状，分别用于测量电和热输运性能。

1.2 结构表征

使用粉末 X 射线衍射(XRD，SmartLab，日本东京 Rigaku 公司)对材料的物相组成进行表征，采用 Cu K_α 辐射(波长 λ=0.154186 nm)作为辐射源。采用装配背散射电子(BSE)探测器和能量色散光谱(EDS)探测器的扫描电子显微镜(SEM，JSM-IT800，日本)表征材料的显微结构。材料晶格参数基于 XRD 衍射数据通过 Fullprof 软件 Rietveld 精修得到。

1.3 电热输运和磁学性能测试

采用标准四探针法(CTA-3，北京 Cryoall 科学与技术有限公司)在氦气氛围中同时测量 σ 和 α，温度范围为 300~750 K。κ 通过公式 $\kappa=\lambda\rho C_p$ 计算得到，其中体积密度(ρ)通过 Archimedes 法测得，比热容(C_p)通过 Dulong-Petit 定律得到，热扩散系数(λ)采用激光闪光法(LFA-467，德国 Netzsch 公司)测量。κ_C 根据 Wiedemann-Franz 定律 $\kappa_C=L\sigma T$ 计算得到，其中 L 为 Lorentz 常数，取值 2.45×10^{-8} $V^2·K^{-2}$。磁滞回线(M–H 曲线)和磁热曲线(M–T 曲线)使用 VersaLab 振动样品磁强计(VSM)模块(美国 Quantum Design 公司)测量。磁熵变曲线(ΔS–T)利用 Maxwell 关系计算得出。

2 结果与讨论

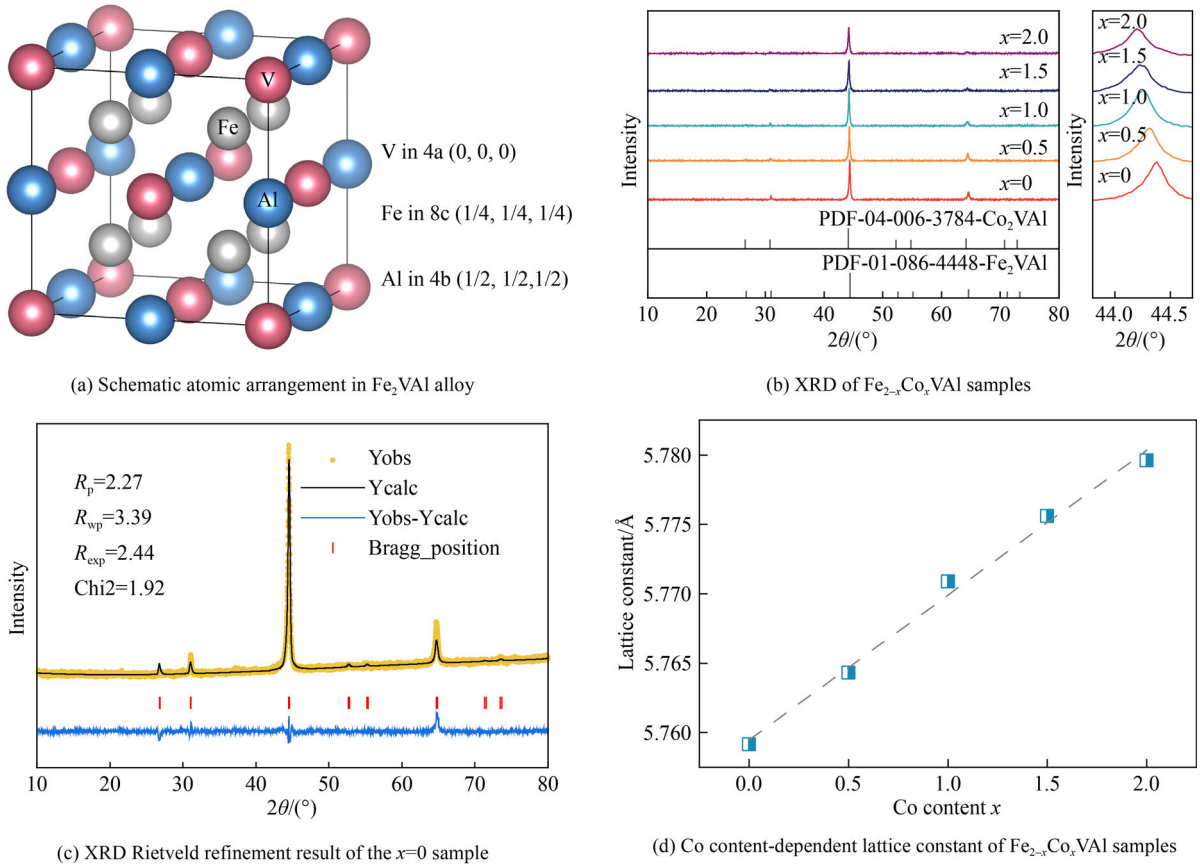
2.1 物相成分

图 1a 为 Fe_2VAl 合金完全有序的 $L2_1$ 晶体结构示意图。该合金空间群为 $Fm\bar{3}m$，过渡金属元素 Fe 和 V 分别占据面心立方晶格的 8c 和 4a 位置，Al 占据 4b 位置。图 1b 为 $Fe_{2-x}Co_xVAl$ 样品的室温 XRD 谱。所有样品的布拉格衍射峰均与 Fe_2VAl 或 Co_2VAl 标准卡片对应，未检测到明显的杂相峰，说明所得块体为单相合金。XRD 谱的局部放大图显示随着 Co 掺量增加，衍射峰逐渐向低角度偏移，表明晶格常数逐渐增加，晶格发生膨胀，物相逐渐由 Fe_2VAl 转变为 Co_2VAl。采用 Fullprof 软件对所有样品进行 Rietveld 精修。图 1c 展示了 x=0 样品的精修结果，图 1c 中实测图谱(黄色圆圈)与计算结果(黑色实线)高度吻合，红色竖线表示布拉格峰的位置，下方的蓝色曲线表示实测图谱与计算谱之间的差异。结构精修所得晶格常数(图 1d)随 Co 掺量增大而增大，与 XRD 结果一致，表明 Co 原子成功取代 Fe 原子。

图 2a~图 2c 分别展示了 x=0、0.5、1.0 样品的背散射电子照片。所有样品均存在不同的衬度。EDS 点分析结果显示样品的实际组成与名义组成非常接近，而不同衬度区域的组成也基本一致。元素面分析结果表明样品中的 Fe、Co、V 和 Al 元素分布均非常均匀，说明材料中的不同衬度并非由成分不同造成，而更可能是源于不同的晶粒取向[32]。

2.2 磁学性能

在 0.1 T 的外加磁场下，测量了所有 $Fe_{2-x}Co_xVAl$ 合金的磁化强度随温度变化的曲线(M–T 曲线)，结果如图 3a 所示。在 50~400 K 测试范围内，随着温度升高，磁化强度逐渐降低。当 Co 掺量 $x\geqslant1.5$ 后，$Fe_{2-x}Co_xVAl$ 样品表现出明显的铁磁–顺磁转变。合金 T_C 可以通过 dM/dT 曲线上的最小值来确定，结果



(a) Schematic atomic arrangement in Fe_2VAl alloy　(b) XRD of $Fe_{2-x}Co_xVAl$ samples

(c) XRD Rietveld refinement result of the x=0 sample　(d) Co content-dependent lattice constant of $Fe_{2-x}Co_xVAl$ samples

图 1　$Fe_{2-x}Co_xVAl$ 样品的晶体结构、XRD 谱、晶体结构精修及晶格常数

Fig. 1　Schematic atomic arrangement, XRD patterns, Rietveld refinement result and lattice constant of $Fe_{2-x}Co_xVAl$ samples

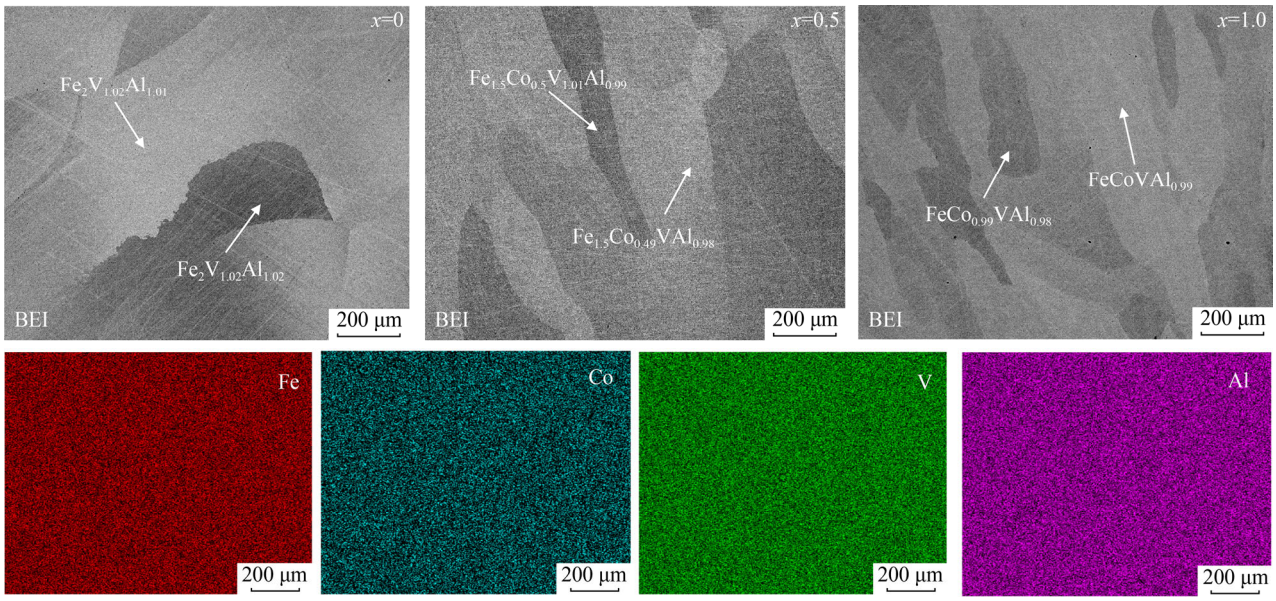


图 2　$Fe_{2-x}Co_xVAl$ 样品的 BSE 照片和 EDS 能谱元素分析

Fig. 2　Backscattered electron images and EDS elemental mapping images of $Fe_{2-x}Co_xVAl$ samples

如图 3b 所示。当 $x \leqslant 1.0$ 时，T_C<50 K，而当 x=1.5 和 2.0 时，T_C 分别可达约 210 K 和 287 K，表明随着 Co 含量的增加，T_C 逐渐增大。实际上，T_C 作为铁磁体宏观磁有序的表征参数，其大小直接反映了体系内交换作用的强度。交换作用越强，自旋平行排列的稳定性越高，需要更大的热扰动才能破坏这种有序态，宏观上表现为更高的 T_C。Bethe–Slater 曲线(图 3c)描述了交换积分(A)与 r_a/r_{3d} 之间的示意

相关性，其中 r_a 和 r_{3d} 分别表示 3d 金属原子与相邻 3d 金属原子的距离和 3d 电子壳层的半径[33]。当 A<0，样品表现为反铁磁性，当 A>0，样品表现为铁磁性。T_C 的大小与交换积分成正相关，在 $Fe_{2-x}Co_xVAl$ 合金中，晶格常数随 Co 含量变化线性变化，原子间距的波动会影响 Fe–Fe、Fe–Co、Co–Co 之间的交换作用。由 Bethe-Slater 曲线的不对称性和 Fe、Co 的相对位置可知，通过改变 Fe 和 Co 的相对含量，曲线会出现交换积分峰值(图中虚线处)[34]，此时 Fe–Co 交换作用可能大于 Co–Co 交换作用和 Fe–Fe 交换作用。这也表明通过优化 $Fe_{2-x}Co_xVAl$ 合金中 Fe 和 Co 的相对含量，有可能取得比全 Fe 和全 Co 基合金更大的 T_C。为此，本工作合成了 $Fe_{0.05}Co_{1.95}VAl$ 合金，发现其 T_C 可大幅增加到 308 K (图 3d)，符合 Bethe–Slater 曲线的变化趋势。这也说明 $Fe_{2-x}Co_xVAl$ 中增强的铁磁性来源于强 Fe–Co 交换作用。

图 3e~图 3f 分别展示了 x=2.0 的样品在 240~340 K 温度范围内(每隔 5 K 测量 1 次)的 Arrott 曲线和 x=1.5，2.0 的样品在 T_C 附近的 Arrott 曲线。根据 Landau 理论，Arrott 曲线斜率为负表示一级磁相变，而斜率为正则表明典型的二级磁相变[35]。x=1.5 和 x=2.0 的样品在 Arrott 图中均呈现正斜率，表面其具有二级磁相变特征。基于经典热力学理论，可以通过磁熵(ΔS)来评估磁制冷效应[36]。根据 Maxwell 关系式 $\Delta S(T,H)=\int_0^H \frac{\mathrm{d}M}{\mathrm{d}T}\mathrm{d}H$，通过磁化法计算了 x=1.5 和 x=2.0 样品的ΔS，并绘制了在不同磁场变化下ΔS 随温度的变化，结果见图 3g~图 3h。ΔS 随测试温度的升高先增加后减少，并在 T_C 处取得峰值。对于 x=1.5 和 2.0 的样品，在 2.5 T 的磁场下ΔS_{max} 分别为 1.04 $J\cdot kg^{-1}\cdot K^{-1}$ 和 0.81 $J\cdot kg^{-1}\cdot K^{-1}$。相对制冷功率(RCP)可用来评估磁制冷材料的制冷能力，采用 $RCP=\Delta S_{max}\times\delta_{FWHM}$ 计算，其中 δ_{FWHM} 是 ΔS–T 曲线的半峰宽[37]。2.5 T 磁场下 x=1.5 和 x=2.0 样品的 RCP 分别约为 71.5 $J\cdot kg^{-1}$ 和 110.7 $J\cdot kg^{-1}$。尽管与经典的磁卡材料 Gd 和 $La(FeSi)_{13}$ 相比，$Fe_{2-x}Co_xVAl$ 合金的磁热性能仍较低，但远高于部分报道的复合热电磁材料，如 MnCoGe/BiSbTe 复合材料(2 T 磁场下ΔS_{max} 为 0.0043 $J\cdot kg^{-1}\cdot K^{-1}$，RCP 为 0.26 $J\cdot kg^{-1}$)和 Gd/BiSbTe 复合材料(2.5 T 磁场下ΔS_{max} 为 0.12 $J\cdot kg^{-1}\cdot K^{-1}$，RCP 为 5.08 $J\cdot kg^{-1}$)[23, 26]，展现出良好的磁热性能。

2.3 电输运性能

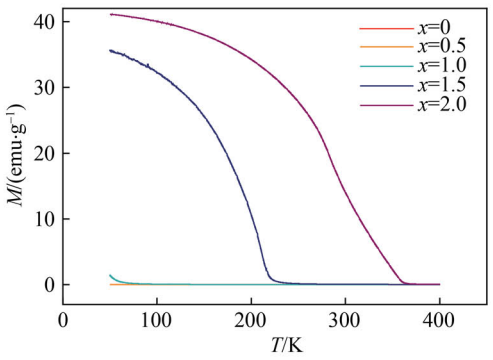
图 4a 显示了 $Fe_{2-x}Co_xVAl$ 样品电导率随温度的变化关系曲线。x=0 样品的电导率 σ 随温度增加而增加，表现出半导体输运行为，这与其窄带隙半金属特性有关[38]。掺杂 Co 原子后，σ 随温度升高而降低，表现出典型的金属导电特性。Co 原子比 Fe 原子多一个价电子，Co 取代 Fe 后载流子浓度显著上升[39]，导致 σ 显著增大。x=2.0 的样品在 300 K 取得最大 σ，达到 4.2×10^5 $S\cdot m^{-1}$，与未掺杂样品相比，提升了约 4.5 倍。所有样品的 α 随温度的变化趋势如图 4b 所示。x=0 的样品在室温时 α 为正值，表现出 p 型传导特征，表明多数载流子是空穴。随着温度升高，α 先逐渐增大，约 400 K 时取得最大值为 17 μV/K，之后由于本征激发效应逐渐降低，并在 700 K 时发生 p–n 转变。掺杂后所有样品的 α 均为负值，表现出 n 型传导特征，这是由于 Co 取代 Fe 引入额外电子，多数载流子从空穴转变为电子。相较于 x=0 的样品，Co 的引入使得 α 峰值往高温区移动。当 x=0.5 时，在 550 K 时 α 最大，为–68 μV/K，其绝对值相比于 x=0 的样品，提升了约 3 倍。通常，对于金属或简并半导体[40]，α 值由式(1)可得。

$$\alpha=\frac{8\pi^2k_B^2}{3eh^2}m^*T\left(\frac{\pi}{3n}\right)^{2/3} \tag{1}$$

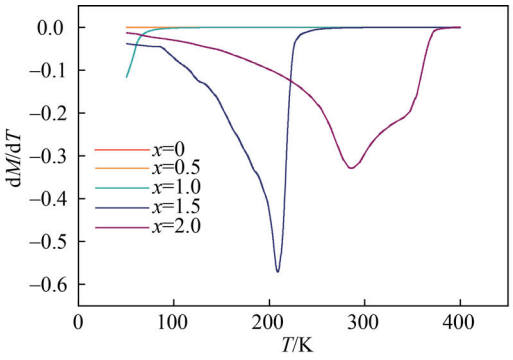
式中：k_B、e、h、m^*和 n 分别代表 Boltzmann 常数、电子电荷、Planck 常数、态密度有效质量和载流子浓度。根据 Mott 热电势理论[41]，α 的增大归因于费米能级附近电子态密度(DOS)的大幅变化。根据文献报道[42]，x=0.5 样品的 DOS 比 x=0 样品的 DOS 具有更加陡峭的斜率，从而具有更大的 m^*，并导致 α 显著增加。进一步增大 Co 的掺量后，由于载流子浓度增大，α 出现明显降低，当 x=2.0 时，α 在室温时降低至–29 μV/K。所有样品的功率因子 $\alpha^2\sigma$ 随温度的变化趋势如图 4c 所示，得益于 α 和 σ 协同增加，x=0.5 样品的 $\alpha^2\sigma$ 在 550 K 时达到最高值，约为 1.14 $mW\cdot K^{-2}\cdot m^{-1}$，与未掺杂样品相比，提升了约 58 倍。

2.4 热输运性能和 zT 值

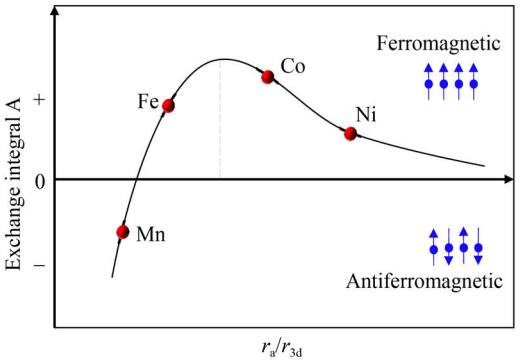
图 5a 是 $Fe_{2-x}Co_xVAl$ 样品的热导率随温度变化关系曲线。由图 5a 可见，在测试温度范围内，随着 x 的增大，κ 逐渐降低，x=2.0 样品具有最低的 κ，300 K 时为 7.1 $W\cdot m^{-1}\cdot K^{-1}$，远低于 x=0 样品在 300 K 时的 28.1 $W\cdot m^{-1}\cdot K^{-1}$。图 5b 是 $Fe_{2-x}Co_xVAl$ 样品的载流子热导率随温度变化的关系曲线。所有



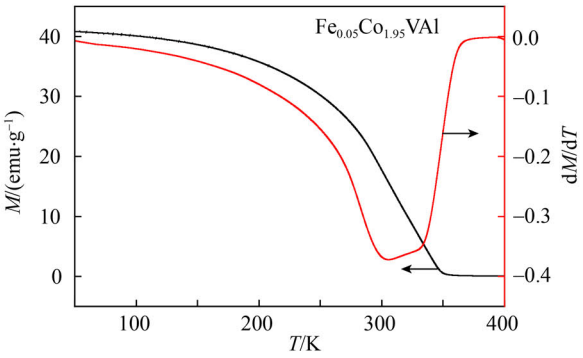
(a) M–T curves



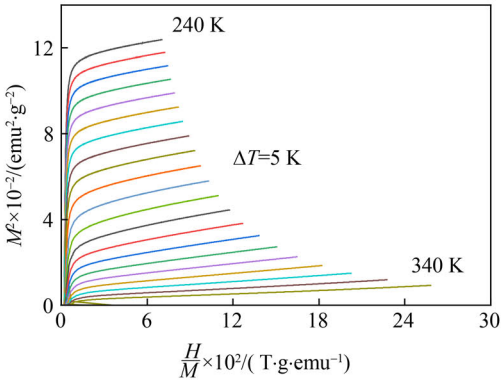
(b) Derivative of magnetization with respect to temperature



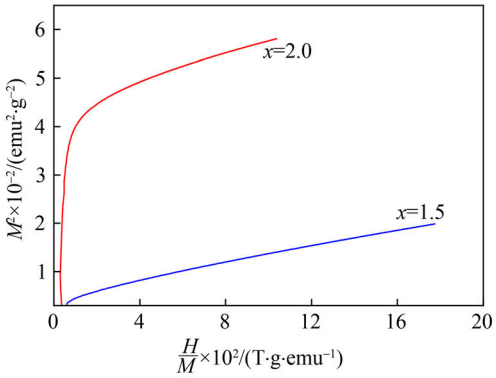
(c) Bethe-Slater curve



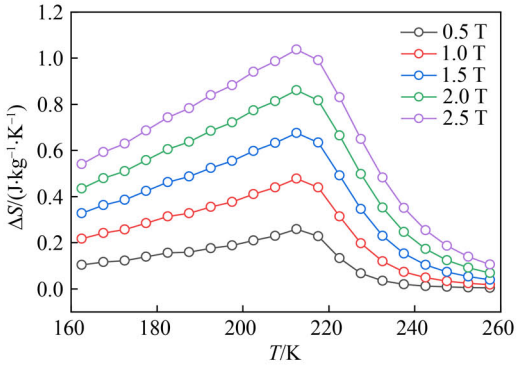
(d) M–T curve and corresponding differential curve of x=1.95



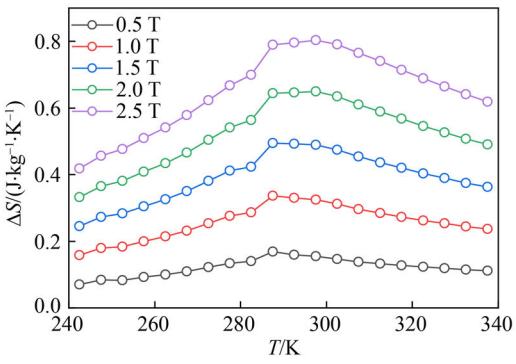
(e) Arrott curves of x=2.0 sample measured in the temperature range of 240–340 K, with a 5 K interval



(f) Arrott curves of x=1.5 and x=2.0 samples near their curie temperature



(g) ΔS as a function of temperature of x=1.5 sample under different magnetic fields

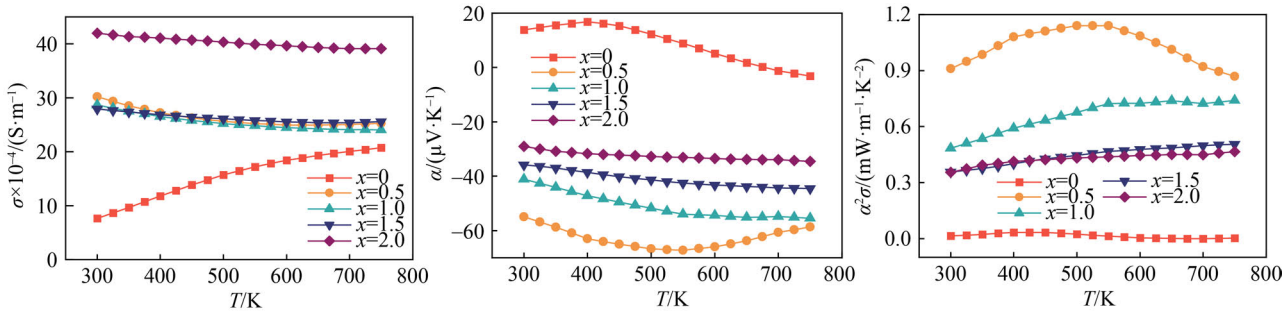


(h) ΔS as a function of temperature of x=2.0 sample under different magnetic fields

Note: 1 emu=10^{-3} A·m^2; M is magnetization; T is temperature; H is magnetic field; ΔS is magnetic entropy change; ΔT is temperature difference for each curve in fig. 3e.

图 3　$Fe_{2-x}Co_x$ VAl 样品的磁学性能

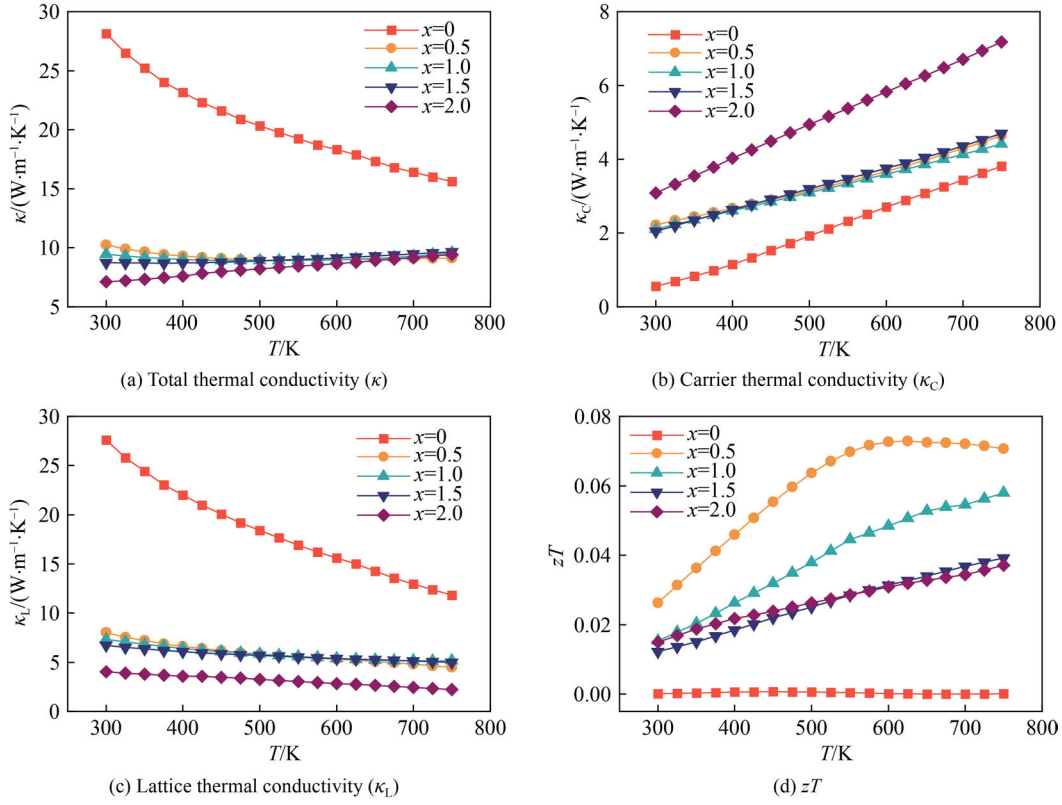
Fig. 3　Magnetic properties of $Fe_{2-x}Co_x$ VAl samples



(a) Electrical conductivity (σ) (b) Seebeck coefficient (α) (c) Power factor ($\alpha^2\sigma$)

图 4 $Fe_{2-x}Co_xVAl$ 样品的电输运性能

Fig. 4 Electrical transport properties of $Fe_{2-x}Co_xVAl$ samples



(a) Total thermal conductivity (κ) (b) Carrier thermal conductivity (κ_C)

(c) Lattice thermal conductivity (κ_L) (d) zT

图 5 $Fe_{2-x}Co_xVAl$ 样品的热输运性能与 zT 值

Fig. 5 Thermal properties and zT values of $Fe_{2-x}Co_xVAl$ samples

样品的 κ_C 随温度升高而升高。随着 x 的增大，κ_C 大幅增加，这归因于电导率的大幅增加。κ_L 由公式 $\kappa_L=\kappa-\kappa_C$ 计算得到，如图 5c 所示。由于声子散射作用随着温度的升高逐渐增强，所有样品的 κ_L 随温度升高逐渐降低。随着 x 的增大，κ_L 显著降低，x=2.0 样品具有最低的 κ_L，在 750 K 时仅为 2.2 $W\cdot m^{-1}\cdot K^{-1}$，与 x=0 样品相比下降了 81.3%。κ_L 的显著降低是由于 Fe 原子和 Co 原子之间的质量波动和半径差异引起强烈的点缺陷散射[43, 44]。图 5d 是 $Fe_{2-x}Co_xVAl$ 样品的 zT 值随温度变化的关系曲线。x=0.5 的样品因具有最大的功率因子和较低的热导率，zT 值最大，在 600 K 时达到 0.073，是 x=0 样品的 260 倍。一般来说，Fe_2VAl 基合金容易在室温附近取得最大值[45]。本工作中，$Fe_{2-x}Co_xVAl$ 合金的最大 zT 值出现在 600 K，这主要归因于 Co 取代 Fe 后在高温区取得了相对较高的综合电性能。尽管目前 $Fe_{2-x}Co_xVAl$ 合金的 zT 值与其他经典热电材料相比仍处于较低水平，但远高于目前报道的其他本征磁性材料，如 $Cr_{0.91}Te_{0.9}Sb_{0.1}$ (300 K 时 zT=0.02)[46]、$CeCrGe_3$ (300 K 时 zT=0.005)[47] 和 $Ce_5Ni_2Si_3$ (300 K 时 zT=0.0014)[48]。

3　结论

系统研究了 Co 掺杂对 Fe_2VAl 基全哈斯勒合金物物相组成、显微结构、磁热性能和热电性能的影响。研究发现，所有的 $Fe_{2-x}Co_xVAl$ 合金为单相化合物，Co 原子成功取代晶格中的 Fe 原子。由于强 Fe–Co 交换作用，Co 掺杂后 T_C 急剧增加。x=1.5 和 2.0 的样品 T_C 分别可达 210 K 和 287 K，在 2.5 T 磁场下 ΔS_{max} 分别可达 1.04 $J·kg^{-1}·K^{-1}$ 和 0.81 $J·kg^{-1}·K^{-1}$，RCP 分别约为 71.5 $J·kg^{-1}$ 和 110.7 $J·kg^{-1}$。Co 取代 Fe 后，合金电导率大幅增加，Seebeck 系数明显增大，功率因子显著提升，x=0.5 的样品具有最高的功率因子，550 K 时达到 1.14 $mW·K^{-2}·m^{-1}$，与未掺杂样品相比，提升了约 58 倍。同时，Co 掺杂后声子散射显著增强，导致晶格热导率大幅降低，并最终导致 zT 大幅提升。x=0.5 的样品具有最大的 zT 值，600 K 时可达 0.073，比未掺杂的 Fe_2VAl 提高了约 260 倍。

参考文献:

[1] GRECO A, APREA C, MAIORINO A, et al. A review of the state of the art of solid-state caloric cooling processes at room-temperature before 2019[J]. Int J Refrig, 2019, 106: 66–88.

[2] LLOPIS R, SÁNCHEZ D, SANZ-KOCK C, et al. Energy and environmental comparison of two-stage solutions for commercial refrigeration at low temperature: Fluids and systems[J]. Appl Energy, 2015, 138: 133–142.

[3] TAKEUCHI I, SANDEMAN K. Solid-state cooling with caloric materials[J]. Phys Today, 2015, 68(12): 48–54.

[4] FRANCO V, BLÁZQUEZ J S, IPUS J J, et al. Magnetocaloric effect: From materials research to refrigeration devices[J]. Prog Mater Sci, 2018, 93: 112–232.

[5] LAGHZAL F, MBAIRI S I, TIHANE A, et al. Comprehensive overview on thermoelectricity −Materials, applications and recent advances[J]. Mater Sci Eng B, 2024, 307: 117512.

[6] LYUBINA J. Magnetocaloric materials for energy efficient cooling[J]. J Phys D Appl Phys, 2017, 50(5): 053002.

[7] ZHANG X, ZHAO L D. Thermoelectric materials: Energy conversion between heat and electricity[J]. J Materiomics, 2015, 1(2): 92–105.

[8] CHEN J C, ZHOU Y H, WANG H J, et al. Comparison of the optimal performance of single- and two-stage thermoelectric refrigeration systems[J]. Appl Energy, 2002, 73(3–4): 285–298.

[9] 白树林, 秦炳超, 赵立东. 载流子迁移率在解耦电–声输运矛盾中的作用[J]. 硅酸盐学报, 2025, 53(4): 733–741.
BAI Shulin, QIN Bingchao, ZHAO Lidong. J Chin Ceram Soc, 2025, 53(4): 733–741.

[10] NIU X, YU J L, WANG S Z. Experimental study on low-temperature waste heat thermoelectric generator[J]. J Power Sources, 2009, 188(2): 621–626.

[11] RIFFAT S B, MA X L. Thermoelectrics: A review of present and potential applications[J]. Appl Therm Eng, 2003, 23(8): 913–935.

[12] MATSUMOTO K, HASEGAWA H, HORIE M, et al. Thermal and electrical conductivity of magnetic refrigerant holmium diboride for magnetic refrigerator application[J]. Cryogenics, 2025, 146: 104020.

[13] PFEUFFER L, LEMKE J, SHAYANFAR N, et al. Microstructure engineering of metamagnetic Ni-Mn-based Heusler compounds by Fe-doping: A roadmap towards excellent cyclic stability combined with large elastocaloric and magnetocaloric effects[J]. Acta Mater, 2021, 221: 117390.

[14] SINGH S, CARON L, D'SOUZA S W, et al. Large magnetization and reversible magnetocaloric effect at the second-order magnetic transition in heusler materials[J]. Adv Mater, 2016, 28(17): 3321–3325.

[15] STEYERT W A. Stirling-cycle rotating magnetic refrigerators and heat engines for use near room temperature[J]. J Appl Phys, 1978, 49(3): 1216–1226.

[16] FORTKAMP F P, LANG G B, LOZANO J A, et al. Design trade-offs for an active magnetic regenerator device[J]. Appl Therm Eng, 2020, 165: 114467.

[17] RICHARD M A, ROWE A M, CHAHINE R. Magnetic refrigeration: Single and multimaterial active magnetic regenerator experiments[J]. J Appl Phys, 2004, 95(4): 2146–2150.

[18] TEYBER R, TREVIZOLI P V, CHRISTIAANSE T V, et al. Performance evaluation of two-layer active magnetic regenerators with second-order magnetocaloric materials[J]. Appl Therm Eng, 2016, 106: 405–414.

[19] YUAN L F, LIU Y, YU J L, et al. Experimental study on cooling performance of active magnetic regenerators with different structures[J]. Int J Refrig, 2023, 153: 184–193.

[20] DE VRIES W, VAN DER MEER T H. Application of Peltier thermal diodes in a magnetocaloric heat pump[J]. Appl Therm Eng, 2017, 111: 377–386.

[21] EGOLF P W, GRAVIER L, FRANCFORT T, et al. High-frequency magnetocaloric modules with heat gates operating with the Peltier effect[J]. Int J Refrig, 2014, 37: 176–184.

[22] MONFARED B. Simulation of solid-state magnetocaloric refrigeration systems with Peltier elements as thermal diodes[J]. Int J Refrig, 2017, 74: 324–332.

[23] LI L Z, WEI P, KE B, et al. Optimizing magnetocaloric and thermoelectric performance of MnCoGe/BiSbTe composites by regulating magnetostructural transition and element diffusion[J]. Mater Charact, 2023, 199: 112760.

[24] LIU C S, LIANG D, CHEN T T, et al. Optimizing room-temperature thermoelectric and magnetocaloric performance *via* constructing multi-scale interfacial phases in LaFeSi/BiSbTe thermo-electro-magnetic refrigeration materials[J]. Adv Funct Mater, 2025, 35(7): 2415368.

[25] ZHU J S, MIAO P L, LI R C, et al. Engineering the thermoelectric and magnetocaloric performance of $Bi_{0.4}Sb_{1.6}Te_3$–Cr_5Te_6 composites[J]. ACS Appl Energy Mater, 2025, 8(7): 4759–4766.

[26] WEI P, KE B, XING L, et al. Atomic-resolution interfacial structures and diffusion kinetics in $Gd/Bi_{0.5}Sb_{1.5}Te_3$ magnetocaloric/thermoelectric composites[J]. Mater Charact, 2020, 163: 110240.

[27] GARMROUDI F, PARZER M, RISS A, et al. Solubility limit and annealing effects on the microstructure & thermoelectricproperties of $Fe_2V_{1-x}Ta_xAl_{1-y}Si_y$ heusler compounds[J]. Acta Mater, 2021, 212: 116867.

[28] GALANAKIS I, DEDERICHS P H, PAPANIKOLAOU N. Slater-Pauling behavior and origin of the half-metallicity of the

full-Heusler alloys[J]. Phys Rev B, 2002, 66(17): 174429.
[29] WANG L Y, DONG Z R, TAN S H, et al. Discovery of a slater–Pauling semiconductor $ZrRu_{1.5}Sb$ with promising thermoelectric properties[J]. Adv Funct Mater, 2022, 32(25): 2200438.
[30] FECHER G H, KANDPAL H C, WURMEHL S, et al. Slater-Pauling rule and Curie temperature of Co_2-based Heusler compounds[J]. J Appl Phys, 2006, 99(8): 08J106.
[31] MIURA Y, SHIRAI M, NAGAO K. *Ab initio* study on stability of half-metallic co-based full-Heusler alloys[J]. J Appl Phys, 2006, 99(8): 08J112.
[32] DIACK-RASSELIO A, ROULEAU O, COULOMB L, et al. Influence of self-substitution on the thermoelectric Fe_2VAl heusler alloy[J]. J Alloys Compd, 2022, 920: 166037.
[33] HU Q, WANG J M, YAN Y H, et al. Invar effect of Fe-based bulk metallic glasses[J]. Intermetallics, 2018, 93: 318–322.
[34] PANDA A K, KUMARI S, CHATTORAJ I, et al. Effect of Fe addition on the crystallization behaviour and Curie temperature of CoCrSiB-based amorphous alloys[J]. Philos Mag, 2005, 85(17): 1835–1845.
[35] MORENO-RAMÍREZ L M, LAW J Y, BORREGO J M, et al. First-order phase transition in high-performance $La(Fe, Mn, Si)_{13}H$ despite negligible hysteresis[J]. J Alloys Compd, 2023, 950: 169883.
[36] SHAO Y Y, MIAO X F, ZHANG Y J, et al. An in-depth review of La–Fe–Si magnetocaloric composites: Structure design and performance enhancement[J]. J Magn Magn Mater, 2022, 564: 170057.
[37] SHEN B G, SUN J R, HU F X, et al. Recent progress in exploring magnetocaloric materials[J]. Adv Mater, 2009, 21(45): 4545–4564.
[38] BERCHE A, NOUTACK M T, DOUBLET M L, et al. Unexpected band gap increase in the Fe_2VAl Heusler compound[J]. Mater Today Phys, 2020, 13: 100203.
[39] LI Y Q, WANG H W, CUI W J, et al. Simultaneous enhancement of electron and phonon transport properties *via* magnetism phase transition in $Fe_xCo_{2-x}TiGe$ heusler alloy[J]. Small, 2025, 21(21): 2500154.
[40] SNYDER G J, TOBERER E S. Complex thermoelectric materials[J]. Nat Mater, 2008, 7(2): 105–114.
[41] HINTERLEITNER B, KNAPP I, PONEDER M, et al. Thermoelectric performance of a metastable thin-film Heusler alloy[J]. Nature, 2019, 576(7785): 85–90.
[42] JAIN V K, JAIN V, LAKSHMI N, et al. Induced spin polarization in Fe_2VAl by substitution of Co at Fe site[J]. Comput Mater Sci, 2015, 108: 56–61.
[43] LIU C, MORELLI D T. Low-temperature thermoelectric properties of Fe_2VAl with partial cobalt doping[J]. J Electron Mater, 2012, 41(6): 1632–1635.
[44] LU W J, ZHANG W Q, CHEN L D. Thermoelectric properties of $(Fe_{1-x}Co_x)_2VAl$ Heusler-type compounds[J]. J Alloys Compd, 2009, 484(1–2): 812–815.
[45] LUE C S, CHEN C F, LIN J Y, et al. Thermoelectric properties of quaternary heusler alloys $Fe_2VAl_{1-x}Si_x$[J]. Phys Rev B, 2007, 75(6): 064204.
[46] GONG Y, SUN J C, HU W W, et al. CrTe as a versatile thermoelectromagnetic multi-functional material[J]. Appl Phys Lett, 2022, 120(2): 023905.
[47] SYNORADZKI K, DAS D, FRĄCKOWIAK A, et al. Study on magnetocaloric and thermoelectric application potential of ferromagnetic compound $CeCrGe_3$[J]. J Appl Phys, 2019, 126(7): 075114.
[48] KOWALCZYK A, FALKOWSKI M, TOLIŃSKI T. Magnetic, transport and thermodynamic properties of $Ce_5Ni_2Si_3$ compound[J]. Solid State Sci, 2012, 14(10): 1496–1502.

Thermoelectric and Magnetocaloric Properties of Co-Doped Fe_2VAl Full-Heusler Alloy at Fe Site

ZHOU Long[1], *YU Jian*[2], *LIANG Dong*[1], *YE Xianfeng*[1], *HE Danqi*[1], *NIE Xiaolei*[1], *WEI Ping*[1], *ZHAO Wenyu*[1], *ZHANG Qingjie*[1]
(1. State Key Laboratory of Advanced Technology for Materials Synthesis and Processing, Wuhan University of Technology, Wuhan 430070, China; 2. School of Materials Science and Engineering, Jiujiang University, Jiujiang 332005, Jiangxi, China)

Extended Abstract

Introduction The demand for refrigeration has substantially increased since 1990s. The refrigerants employed in conventional cooling systems are known to cause ozone depletion and subsequent environmental impacts. Thermoelectric (TE) cooling and magnetocaloric (MC) cooling technologies face some challenges in replacing conventional vapor compression systems due to their relatively low coefficients of performance (COP) and heat transfer efficiency. A combination of TE and MC cooling could be a promising way to improve the heat-exchange efficiency. Recent studies have focused extensively on thermo-electro-magnetic materials that simultaneously exhibit TE and MC properties. These materials include both MC/TE composites and intrinsic thermo-electro-magnetic materials. However, inherent heterogeneous interfacial reactions in MC/TE composites simultaneously degrade both MC and TE performance. Intrinsic thermo-electromagnetic materials as single-phase compounds can effectively avoid such a degradation. Fe_2VAl-based Heusler alloys exhibit promising thermoelectric properties due to their unique electronic structure. The incorporation of magnetic Co atoms is expected to simultaneously enhance the Curie temperature (T_C), and synergistically regulate both MC and TE properties in Fe_2VAl-based Heusler compounds. This study prepared a series of $Fe_{2-x}Co_xVAl$ alloys *via* arc-melting and characterized their phase composition, MC properties, and TE performance. This study demonstrated that controlled Co doping could be critical for optimizing the thermo-electro-magnetic properties of intrinsic $Fe_{2-x}Co_xVAl$ alloys, thus providing an effective material design strategy for solid-state hybrid MC/TE cooling technologies.

Methods A series of $Fe_{2-x}Co_xVAl$ (x = 0, 0.5, 1.0, 1.5, 2.0) ingots were prepared *via* arc melting in argon (Ar) atmosphere with high

purity Fe (99.99%, blocks), Co (99.9%, pieces), V (99.95%, pieces), and Al (99.99%, granules). To ensure a homogeneity, the ingots were subjected to five remelting cycles with intermediate flipping. The ingots were cut into desired shapes using wire electrical discharge machining for the measurement of thermal and electrical transport properties. The phase structure of the materials was determined by powder X-ray diffraction (XRD, SmartLab, Rigaku Co., Japan). The microstructures were determined by scanning electron microscopy (JSM-IT800, Japan) equipped with a back-scattered electron detector and a Bruker energy-dispersive spectroscopy detector. The lattice constants were refined according to the Rietveld method using the Fullprof program. The Seebeck coefficient (α) and electrical conductivity (σ) were measured simultaneously by a standard four-probe method (CTA-3, Beijing Cryoall Science and Technology Co., Ltd., China) in a helium atmosphere at 300–750 K. The thermal diffusivity (λ) was measured by a laser flash method (Netzsch LFA-467, Netzsch Co., Germany). The thermal conductivity was calculated according to $\kappa = \lambda\rho C_p$, where C_p was the heat capacity according to the Dulong-Petit formula, and the density ρ was measured based on the Archimedes prinicple. The magnetization versus magnetic field (M–H) curves and thermomagnetic (M–T) curves were measured with a multi-VersaLab vibrating sample magnetometer (VSM, VersaLab, Quantum Design INC., USA). The magnetic entropy change curves (ΔS–T) were calculated using the Maxwell relations.

Results and discussion The results indicate that the incorporation of the magnetic element Co into Fe_2VAl Heusler alloy can synergistically regulate its MC and TE properties, showing a potential to become a high-performance intrinsic thermo-electro-magnetic material. The XRD patterns show that the Bragg diffraction peaks of all the samples match the standard cards without impurity peaks detected. The lattice constant increases with the increase of Co doping, indicating the continuous substitution of atoms Fe by atoms Co. The SEM images reveal that Fe, V, and Al are homogeneously distributed in the materials without any impurity phases. The incorporation of Co significantly elevates the T_C of Fe_2VAl-based Heusler alloys to industrially viable ranges, which is consistent with the Slater-Pauling rule predictions and the Bethe-Slater curve validation. At a magnetic field of 2.5 T, the maximum magnetic entropy change (ΔS_{max}) increases to 1.04 $J\cdot kg^{-1}\cdot K^{-1}$ for the sample with x of 1.5 $J\cdot kg^{-1}\cdot K^{-1}$ and 0.81 $J\cdot kg^{-1}\cdot K^{-1}$ for the sample with x of 2.0. The sample with x of 2.0 achieves an enhanced relative cooling power (RCP) of 110.7 $J\cdot kg^{-1}$, benefiting from its significantly broadened full-width at half-maximum (δ_{FWHM}). The introduction of Co significantly increases the electrical conductivity (σ), shifting a transport behavior from semiconducting to metallic. The σ of the sample with x of 2.0 is the maximum vaule of 4.2×10^5 $S\cdot m^{-1}$ at 300 K. The substitution of Co introduces extra electrons, switching the Seebeck coefficient (α) from positive to negative values, indicating that the majority carriers shift from holes to electrons. The α of the sample with x of 0.5 is the maximum vaule of –68 μV/K at 550 K. The sample with x of 0.5 sample exhibits a peak power factor ($\alpha^2\sigma$) of 1.14 $mW\cdot K^{-2}\cdot m^{-1}$ at 550 K. The decrease in $\alpha^2\sigma$ at high temperatures is due to the combined effects of reduced electrical conductivity and the decrease in the Seebeck coefficient caused by intrinsic excitation. At 300 K, The lattice thermal conductivity of the sample with x of 2.0 is the minimum value of 4.1 $W\cdot m^{-1}\cdot K^{-1}$. The maximum zT value reaches 0.073 K at 600 K for the sample with x of 0.5, which is 260 times higher than that of the sample with x of 0.

Conclusions The introduction of the magnetic element Co could synergistically regulate the magnetocaloric and thermoelectric properties of Fe_2VAl Heusler alloy. The sharp increase in T_C could be attributed to the intense Fe–Co exchange interaction. The sample with x of 1.5 had the ΔS_{max} of 1.04 $J\cdot kg^{-1}\cdot K^{-1}$. The sample with x of 2.0 had the maximum RCP of 110.7 $J\cdot kg^{-1}$. The sample with x of 0.5 had the maximum zT value of 0.073 at 600 K. The existing research showed that the T_C could be further increased and a better balance between MC and TE properties could be achieved *via* optimizing the Co doping content. To further enhance the TE performance without affecting T_C, doping heavy elements at the V site to increase phonon scattering or introducing V/Al antisite defects to improve electrical transport properties could be considered. This work could provide an effective material design strategy for developing intrinsic thermo-electro-magnetic materials based on Full Heusler alloys.

Keywords thermo-electro-magnetic materials; full-heusler alloys; magnetocaloric performance; thermoelectric performance